

- 1 The general formulation for mean annual runoff components
- 2 estimation and their change attribution ~~at mean annual time~~
- 3 ~~scale~~

Yufen He¹, Changming Li^{1*}, Hanbo Yang^{1*}

5 1 State Key Laboratory of Hydroscience and Engineering, Department of Hydraulic Engineering,
6 Tsinghua University, Beijing 100084, China

*Correspondence: Changming Li (licm_13@163.com), Hanbo Yang (yanghanbo@tsinghua.edu.cn)

9 Abstract

10 Estimating runoff components, including surface flow, baseflow and total runoff is essential for
11 understanding precipitation partition and runoff generation and facilitating water resource
12 management. However, a general framework to quantify and attribute runoff components is still
13 lacking. Here, we propose a general formulation through observational data analysis and
14 theoretical derivation based on the two-stage Ponce-Shetty model (named as the MPS model).
15 The MPS model characterizes mean annual runoff components as a function of available water
16 with one parameter. The model is applied over 662 catchments across China and the contiguous
17 United States. Results demonstrate that the model well depicts the spatial variability of runoff
18 components with R^2 exceeding 0.81, 0.44 and 0.80 for fitting surface flow, baseflow and total
19 runoff, respectively. The model effectively simulates multi-year runoff components with R^2
20 exceeding 0.97, and the proportion of runoff components relative to precipitation with R^2
21 exceeding 0.94. By using this conceptual model, we elucidate the responses of surface flow and
22 baseflow to available water and environmental factors for the first time. The surface flow is
23 jointly controlled by precipitation and environmental factors, while baseflow is mainly influenced
24 by environmental factors in most catchments. The universal and concise MPS model offers a new
25 perspective on the long-term catchment water balance, facilitating broader application in
26 large-sample investigations without complex parameterizations and providing an efficient tool to
27 explore future runoff variations and responses under changing climate.

28 **Key Points**

29 (1) A general and concise formulation is proposed to quantify, and attribute mean annual
30 surface flow, baseflow and total runoff.

31 (2) The formulation characterizes runoff components as a function of available water without
32 additional and complicated parameter calculation.

33 (3) The formulation performs well in quantifying and attributing runoff components in 662
34 catchments.

35 **1. Introduction**

36 Runoff is the primary freshwater resource accessible for human life and plays an essential role
37 in the water cycle (He et al., 2022; Wang et al., 2024). Based on the propagation time and
38 hydraulic response of a catchment, total runoff (Q) can be divided into baseflow (Q_b) and surface
39 flow (Q_s) (Gnann et al., 2019; Singh et al., 2019). Baseflow, also referred to as slow flow, is
40 defined as the flow that originates from groundwater and other delayed sources (such as wetlands,
41 lakes, snow and ice), and generally sustains streamflow during dry periods (Gnann, 2021; Hall,
42 1968). Baseflow is the relatively stable component of runoff, playing a vital role in aquatic
43 ecosystems (de Graaf et al., 2019; Price et al., 2011), water quality (Ficklin et al., 2016) and
44 sustained water supplies (Fan et al., 2013). Surface flow, also referred to as fast flow, results from
45 rapid processes like the saturation or infiltration of excess overland flow and swift subsurface
46 flow (Beven and Kirkby, 1979), leading to immediate water movement. Surface flow occurs more
47 rapidly and with more drastic changes than baseflow, which is primarily responsible for flood
48 generation (Yin et al., 2018) and soil erosion (Morgan, 2011).

49 Most current studies focus on total runoff variability and attribution, and the relevant
50 researches are fairly mature (Berghuijs et al., 2017; Han et al., 2023; Liu et al., 2021). However,
51 few studies pay attention to comprehensive research on the different runoff components (Li et al.,
52 2020; Liu et al., 2019), and the attributions of Q_s and Q_b changes are still unclear (Hellwig and
53 Stahl, 2018). Baseflow and surface flow represent different hydrological processes, and their
54 implications for watershed management are also not identical (Zheng Mingguo, 2014). For

55 example, the research conducted by Ficklin et al. (2016) in the United States points out apparent
56 spatial differences between Q_b and Q_s in different seasons. Therefore, it is necessary to quantify
57 runoff components and distinguish their controlling factors to better understand the runoff
58 dynamics and facilitate water resources management in the context of intensified climate change
59 and anthropogenic disturbance.

60 Unlike Q , which is ascertainable through direct observation at hydrological gauges, Q_b and Q_s
61 can only be estimated through indirect methods, including baseflow separation (Wu et al., 2019;
62 Zhang et al., 2017), isotope tracing (Hale et al., 2022; Wallace et al., 2021) and hydrological
63 modeling (Al-Ghobari et al., 2020; Cheng et al., 2020; Huang et al., 2007; Kaleris and Langousis,
64 2017). The first two methods estimate Q_b initially, and Q_s is then derived as the difference
65 between the Q and the estimated Q_b , limiting their ability to examine the dynamic variations of
66 each runoff component independently, and the isotope tracing method is challenging to conduct
67 on a large and long-term scale. The hydrological modeling enables to simulate Q_b and Q_s
68 separately, typically reflected in different modules and empirical formulations. In hydrological
69 models, Q_b is encoded using linear or non-linear storage-discharge functions (Chen and Ruan,
70 2023; Cheng et al., 2020). Q_s is closely related to rainfall, but the models for estimating it are
71 usually event-based (such as the Soil Conservation Service Curve Number method (Al-Ghobari et
72 al., 2020; SCS, 1972; Shi et al., 2017) and very few studies explored the controls on the mean
73 annual Q_s (Neto et al., 2020). Among various models, the Budyko framework (Budyko, 1974) in
74 conjunction with water-energy balance method (Choudhury, 1999; Yang et al., 2008) (see the
75 second row in Table 1), has been widely used in the analysis of mean annual Q due to its simple,
76 universal and transparent characteristics (He et al., 2022; Roderick and Farquhar, 2011).

77 Recently, utilizing the extended Budyko framework to estimate Q_b and Q_s has attracted
78 attention. Wang and Wu (2013) and Neto et al. (2020) established the regression relationship
79 between baseflow fraction (BFC , the ratio of Q_b to precipitation (P)) and aridity index (ϕ , the
80 ratio of mean annual potential evapotranspiration (E_0) to P) using analytical formulation.
81 However, Gnann et al. (2019) reported that using only the ϕ struggles to delineate baseflow
82 variability in humid catchments, where the impact of soil water storage capacity (S_p) is as critical
83 as that of the ϕ . Thus, Cheng et al. (2021) proposed an analytical curve for describing mean
84 annual Q_b by introducing S_p as another theoretical boundary. Results show that the developed

85 curve agrees well with the observed *BFC* ($R^2 = 0.75$, RMSE = 0.058) and Q_b ($R^2 = 0.86$,
 86 RMSE = 0.19 mm), outperforming the original Budyko framework. Analogously, Yao et al.
 87 (2021) derived similar functions incorporated the ϕ , S_p and a shape parameter to model *BFC* and
 88 baseflow index (*BFI*, the ratio of Q_b to Q). These extended Budyko frameworks accounting for S_p
 89 have advantages in simulating Q_b . However, S_p is challenging to obtain through observations and
 90 often requires calibration (Cheng et al., 2021) or computation (Yao et al., 2021), adding certain
 91 uncertainties to the model. Notably, the calibration performance of Q_s in equation (1) to obtain W_p
 92 (the proxy of S_p) in the catchments of China are not always satisfactory, especially in the northern
 93 catchments (Figure S1). Moreover, the complicated forms can bring inherent uncertainties and
 94 these studies have not validated the formulations of Q_s , which are derived by subtracting Q_b from
 95 Q or fitting curves (Cheng et al., 2021; Neto et al., 2020), implying that they may overlook the
 96 physical processes represented by surface flow. In the subsequent discussion, the Budyko
 97 framework and extended Budyko equations are collectively referred to as the "Budyko-type
 98 formulations" (Table 1).

99 Many researchers have observed similar behavior of Q_b to Q (Cheng et al., 2021; Gnann et al.,
 100 2019; Wang and Wu, 2013). Is there a similar behavior for Q_s ? In a two-stage partitioning theory
 101 (L'vovich, 1979), runoff components are delineated based on the available water at each stage.
 102 Therefore, is there a general framework to unify different runoff components? Although various
 103 functional forms have been proposed for estimating runoff components in the literature, a
 104 universal method that reveals the mechanisms of mean annual runoff components generation and
 105 subsequent quantification and attribution is still in need.

106 **Table 1.** The Budyko-type formulations for estimating mean annual runoff components

References	Formulations	Parameters
Choudhury (1999); Yang et al. (2008)	$Q = P - \frac{P \times E_0}{(P^n + E_0^n)^{1/n}}$	n calibrated
Wang and Wu (2013)	$\frac{Q_b}{P} = 1 - \left[1 + \left(\frac{E_0}{P} \right)^{-v} \right]^{-1/v}$	v fitted
Neto et al. (2020)	$f_s(\phi) = \exp(-\phi^a + \delta_s^b)$ $f_b(\phi) = \exp(-\phi^c + \delta_b^d)$	a, b, c, d $\delta_s = \ln \left(\left[\frac{\bar{Q}_s}{P} \right]_{max} \right)^{1/b}$

带格式的：字体：(默认) Times New Roman, (中文) 宋体, 字体颜色：黑色

带格式的：字体：非倾斜

$$\delta_B = \ln \left(1 - \left[\frac{\bar{Q}_S}{P} \right]_{max} \right)^{1/d}$$

fitted

$$\frac{Q_s}{P} = -\frac{E_0 + S_p}{P} + \left[1 + \left(\frac{E_0 + S_p}{P} \right)^{\alpha_1} \right]^{1/\alpha_1}$$

Cheng et al. (2021)

$$\frac{Q_b}{P} = \frac{S_p}{P} + \left[1 + \left(\frac{E_0}{P} \right)^{\alpha_2} \right]^{1/\alpha_2}$$

S_p, α_1, α_2

calibrated

$$- \left[1 + \left(\frac{E_0 + S_p}{P} \right)^{\alpha_2} \right]^{1/\alpha_2}$$

Q_b

$$= \frac{P + S_b - \sqrt{(P + S_b)^2 - 2aS_bP}}{a} \left[1 \right]$$

Yao et al. (2021)

$$- \frac{1 + \frac{E_0}{P} \frac{P}{S_b} - \sqrt{\left(1 + \frac{E_0}{P} \frac{P}{S_b} \right)^2 - 2a \frac{E_0}{P} \frac{P}{S_b}}}{a} \left[\right]$$

S_b (estimated from

cumulative distribution

function), a (calibrated)

带格式的: 字体: (默认) Times New Roman, (中文) 宋体, 字体颜色: 黑色

带格式的: 字体: 倾斜

$$Q = P - \frac{\frac{P}{S_b} + 1 - \sqrt{\left(\frac{P}{S_b} + 1 \right)^2 - 2a \frac{P}{S_b}}}{a}$$

$$* \frac{E_0 + S_b - \sqrt{(E_0 + S_b)^2 - 2aE_0S_b}}{a}$$

107 Note that P is the mean annual precipitation, E_0 is the mean annual potential evapotranspiration, $f_S(\phi)$ and
108 $f_B(\phi)$ are the surface flow and baseflow function, respectively and S_p is the catchment storage capacity.

109 To address these questions, we derived a modified two-stage partitioning framework through
110 observational data analysis and theoretical derivation based on the Ponce-Shetty model (Ponce
111 and Shetty, 1995; Sivapalan et al., 2011) (namely the MPS model) at mean annual time scale. The
112 Ponce-Shetty model is a conceptual model with physical constraint developed at annual scale to
113 depict how precipitation is partitioned, stored and released in the catchment (Gnann et al., 2019).
114 It posits that annual precipitation is partitioned into Q_s and soil wetting (W) and, subsequently, the
115 resulting W is partitioned into Q_b and vaporization (V) (Sivapalan et al., 2011). The MPS model

116 enables large-sample catchments research, which may lead to new understanding of mean annual
117 water balance and allocation.

118 In general, the objectives of this study are to (1) develop a general and concise formulation to
119 describe runoff components variability at mean annual time scale; (2) validate and compare the
120 performance of the developed formulation against Budyko-type formulations; (3) attribute the
121 variations of runoff components induced by the changes of precipitation and other factors. Here,
122 we modify the Ponce-Shetty model according to some conditions and hypothesize a general
123 runoff components model (the MPS model), that describes Q_s , Q_b and Q as a function of
124 respective available water with one parameter. The MPS model is then validated over 662
125 catchments across China and the contiguous United States (the CONUS) over a wide range of
126 hydro-meteorological circumstances. The performance of the MPS model is also compared with
127 the Budyko-type formulations. Section 2 introduces the derivation of the MPS model. Section 3
128 provides the study catchments, data and the parameter estimation technique. Section 4 shows the
129 results followed by a discussion in Section 5. The conclusions are summarized in Section 6.

130 **2. Derivation of the Modified Ponce-Shetty Model**

131 L'vovich (1979) proposed a conceptual theory for the two-stage catchment water balance
132 partition at the annual time scale according to Horton's approach (Horton, 1933). Firstly,
133 precipitation is partitioned into surface flow (Q_s) and catchment wetting (W , stored water), and
134 then, the catchment wetting is partitioned into baseflow (Q_b) and vaporization (V , including
135 interception loss, evaporation and transpiration). Ponce and Shetty (1995) conceptualized the
136 partition of each step as the form of a competition, and derived the formulations of runoff
137 components based on the proportionality hypothesis. Sivapalan et al. (2011) reintroduced the
138 Ponce-Shetty equations as follows:

139 In the first stage, $P = Q_s + W$:

$$Q_s = \begin{cases} 0, & \text{if } P \leq \lambda_s W_p \\ \frac{(P - \lambda_s W_p)^2}{P + (1 - 2\lambda_s)W_p}, & \text{if } P > \lambda_s W_p \end{cases} \quad (1)$$

W

$$= \begin{cases} P, & \text{if } P \leq \lambda_s W_p \\ P - \frac{(P - \lambda_s W_p)^2}{P + (1 - 2\lambda_s)W_p}, & \text{if } P > \lambda_s W_p \end{cases} \quad (2)$$

$$P \rightarrow \infty, Q_s \rightarrow P - W_p, W \rightarrow W_p \quad (3)$$

140 In the second stage, $W = Q_b + V$:

Q_b

$$= \begin{cases} 0, & \text{if } W \leq \lambda_b V_p \\ \frac{(W - \lambda_b V_p)^2}{W + (1 - 2\lambda_b)V_p}, & \text{if } W > \lambda_b V_p \end{cases} \quad (4)$$

V

$$= \begin{cases} W, & \text{if } W \leq \lambda_b V_p \\ W - \frac{(W - \lambda_b V_p)^2}{W + (1 - 2\lambda_b)V_p}, & \text{if } W > \lambda_b V_p \end{cases} \quad (5)$$

$$W \rightarrow \infty, Q_b \rightarrow W - V_p, V \rightarrow V_p \quad (6)$$

141 where λ_s and λ_b are the surface flow and baseflow initial abstraction coefficients, respectively,
142 which range from 0 to 1. The larger value of λ , the more difficult it is to generate flow. W_p and V_p
143 are catchment wetting potential and vaporization potential, respectively, which are greater than 0.
144 The relative $\lambda_s W_p$ and $\lambda_b V_p$ are the surface flow and baseflow generation thresholds,
145 respectively.

146 Note that the interannual water storage change is supposed to be negligible (Ponce and Shetty,
147 1995). In a companion paper of Sivapalan et al. (2011), Harman et al. (2011) employed the
148 annual Ponce-Shetty model at mean annual time scale and validated its applicability. Using the
149 first phase as an example, Q_s can be considered a function of λ_s , denoted as $f(\lambda_s)$:

$$f(\lambda_s) = \begin{cases} 0, & \text{if } \lambda_s \geq P/W_p \\ \frac{(P - \lambda_s W_p)^2}{P + (1 - 2\lambda_s)W_p}, & \text{if } \lambda_s < P/W_p \end{cases} \quad (7)$$

150 When $\lambda_s < P/W_p$, the Taylor expansion of $f(\lambda_s)$ at $\lambda_s=0$ is:

$$f(\lambda_s) = f(0) + f'(0) * \lambda_s + \frac{f''(0)}{2!} * \lambda_s^2 + \dots + \frac{f^n(0)}{n!} * \lambda_s^n + \dots \quad (8)$$

151 Hence, we have the zeroth-order approximation:

$$f(\lambda_s) \approx \frac{P^2}{P + W_p} \quad (9)$$

152 When the remainder term is relatively small, an approximation equation can be used to
153 estimate the multi-year Q_s as:

$$Q_s = \frac{P^2}{P + W_p} \quad (10)$$

154 In addition, the zeroth-order approximation of Q_b can be similarly obtained as:

$$Q_b = \frac{W^2}{W + V_p} \quad (11)$$

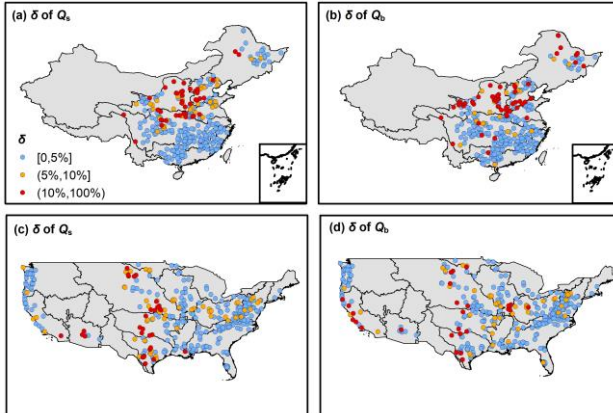
155 To evaluate the impact of the remainder term, we calculate the relative bias (δ) of runoff
156 components for 312 basins in China and 350 basins in the United States using the approximate
157 equations (Eq (10) and Eq (11)) and the original Ponce-Shetty equations (Eq (1) and Eq (4)) (data
158 sources in Section 3.1). The parameters in the original Ponce-Shetty equations are calibrated
159 using the nonlinear least squares method. The δ is calculated as:

$$\delta = \frac{|\widetilde{Q}_y - Q_y|}{Q_y} \quad (12)$$

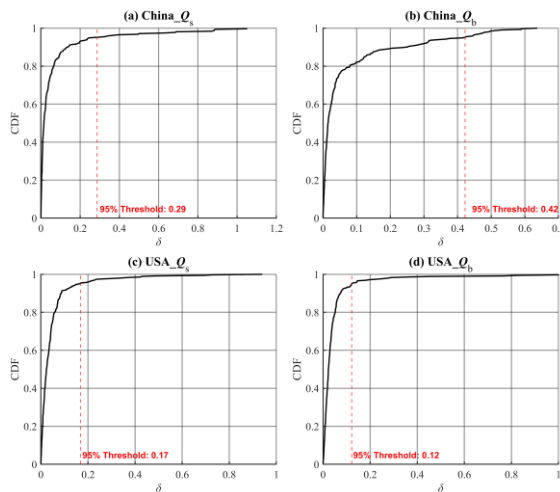
160 where Q_y represents runoff components estimated by the Ponce-Shetty equations, and \widetilde{Q}_y
161 represents runoff components estimated by the approximate equations (Eq (10) and Eq (11)).

162 The spatial distribution of δ and the cumulative distribution functions (CDFs) of δ are
163 shown in Figure 1 and Figure 2, respectively. As shown in Figure 1, 77% of the basins have an δ
164 of less than 5%. The average δ for estimating Q_s is 6.5% in China and 4.8% in the United States,
165 while the average δ for estimating Q_b is 7.9% in China and 6.6% in the United States, with
166 larger deviations observed in arid basins. Figure 2 indicate that the δ values for the approximate
167 model are within acceptable limits across both China and CONUS. The relatively low 95%
168 threshold values, particularly for the USA datasets, suggest that the majority of predictions fall
169 within a narrow error range, indicating robust model performance. This acceptability of δ across
170 regions and variables highlights the approximate equations' capability to maintain prediction

171 accuracy under varying geographical and hydrological conditions, indicating that the Zeroth-order
 172 approximation is representative for the original Ponce-Shetty model.



173
 174 **Figure 1.** The distribution of relative bias (δ) between the results by the approximate equations
 175 (Eq (10) and Eq (11)) versus the original Ponce-Shetty equations (Eq (1) and Eq (4)). The first
 176 row shows the results for 312 basins in China, and the second row shows the results for 350
 177 basins in CONUS. The first column corresponds to surface flow (Q_s), and the second column
 178 corresponds to baseflow (Q_b).



179
 180 **Figure 2.** Cumulative distribution functions (CDFs) of the relative bias (δ) for each dataset,
 181 represented by four subplots corresponding to different regions and variables: (a) China_Qs, (b)

182 China_ Q_b , (c) USA_ Q_s , and (d) USA_ Q_b . Each subplot includes a red dashed line indicating the
183 95% δ threshold

184 Therefore, we can approximately consider that on a multi-year scale, Q_s and Q_b can be
185 estimated using the zeroth-order approximation in Eq (10) and Eq (11). We subsequently assume
186 a similar formulation of mean annual Q :

$$Q = \frac{P^2}{P + U_p} \quad (13)$$

187 where U_p is the parameter representing the upper limit of the portion remaining after precipitation
188 is allocated to runoff, hereafter we refer to U_p as evapotranspiration potential.

189 Integrating equations (10), (11) and (13), we conclude a general formulation to depict
190 multi-year variability of runoff components and their quantification, hereafter referred to as the
191 modified Ponce-Shetty model (the MPS model):

$$Q_y = \frac{X^2}{X + M} \quad (14)$$

192 where Q_y represents runoff components (i.e., Q , Q_s , Q_b), X corresponds to the available water of
193 each runoff component, i.e., P is the available water of Q and Q_s , and W the available water of Q_b .
194 M is an integrated parameter, representing the comprehensive effects of catchment characteristics
195 and atmospheric water and energy demand.

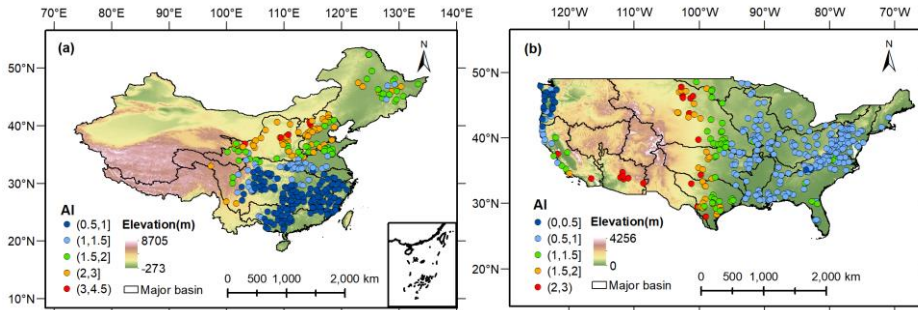
196 The MPS model encodes runoff components as a function of available water with only one
197 parameter, which not only considers processes of runoff generation with physical constraints, but
198 also, compared to the Budyko-type formulations and the original Ponce-Shetty model, is more
199 concise in form and requires fewer parameters. Therefore, it is possible to estimate the long-term
200 runoff components when only long-term variables are known.

201 **3. Data and Methodology**

202 **3.1. Data**

203 To validate the reliability of the MPS model, daily hydrological and meteorological data from
204 312 catchments in China (Li et al., 2024) and 350 catchments in the CONUS are collected. [The](#)

205 criteria for catchments screening can refer to He et al. (2025). The location of all the catchments
206 hydrological stations is shown in Figure 3.



207
208 **Figure 3.** Location of hydrological stations for the (a) 312 catchments in China and (b) 350
209 catchments in the CONUS, colored by the value of aridity index (ϕ , namely E_0/P).

210 In China, precipitation data at 0.25° spatial resolution are obtained from the China
211 Gauge-based Daily Precipitation Analysis (CGDPA) (Shen and Xiong, 2016). Other
212 meteorological data, including wind speed, sunshine hours, relative humidity, and air temperature,
213 are from about 736 stations of the China Meteorological Data Service Center
214 (<http://data.cma.cn/en>, last access: 11 November 2023). The in-site meteorological data are
215 interpolated into a 10-km grid using the inverse-distance weighted method (Yang et al., 2014).
216 We use the Penman equation (Penman, 1948) to estimate E_0 of each grid using standard
217 meteorological inputs (e.g., radiation, humidity, wind, temperature). The Penman equation is
218 widely recommended to estimate E_0 at catchment scale due to its physical basis (Pimentel et al.,
219 2023; Wang et al., 2025), and it provides a consistent reference for our annual, large-sample
220 analyses. The aridity index ϕ is subsequently calculated as E_0/P . All grid data are aggregated
221 and lumped for individual catchments. The discharge data are collected from the Hydrological
222 Bureau of the Ministry of Water Resources of China (<https://www.mwr.gov.cn/english/>, last
223 access: 20 December 2023) and are selected based on the length of records exceeding 35 years
224 with less than 5% missing data. The time range for all data is 1960-2000.

225 In the CONUS, we use data set from CAMELS (Addor et al., 2017; Newman et al., 2015). The
226 CAMELS data set provides 662 catchments with daily time series of precipitation and observed
227 runoff along with aridity index, and most catchments contain 35 years of continuous runoff from

带格式的: 字体: 倾斜

带格式的: 下标

带格式的: 字体: (默认) Times New Roman, (中文) 宋体, 小四, 字体颜色: 黑色

228 1980 to 2014. The criteria for excluding catchments are referred to Gnann et al. (2019), and
229 finally 350 catchments remained.

230 We use the one-parameter Lyne-Hollick digital filter (Lyne, 1979) to separate daily Q_s and Q_b
231 from daily Q . The Lyne-Hollick method is applied forward, backward, and forward again with a
232 filter parameter of 0.925 and has manifested to be reliable to obtain runoff components (Lee and
233 Ajami, 2023). We use the separated Q_s and Q_b as the reference. Although there are other baseflow
234 separation algorithms, according to Troch et al. (2009), the choice of baseflow separation
235 algorithm is not a significant determinant of the water balance at the annual scale.

236 All the hydrological and meteorological data are aggregated to the annual and mean annual
237 time scales for further analysis.

238 **3.2. Calibration and Validation**

239 Spatially, to verify the MPS model's ability to characterize the variability of runoff components
240 between catchments, we utilize the least squares fitting algorithm to estimate parameters, i.e., W_p ,
241 V_p and U_p . The three parameters are restricted to being between 0 mm and 50,000 mm, which is
242 considered high enough to not affect the parameter estimation (Gnann et al., 2019).

243 In terms of time, we split all data into two periods for parameter calibration and validation of
244 Eq. (14) for individual catchments. In China, the data ranges from 1960 to 2000, so we use the
245 first 31 years (1960-1990) as the calibration period and the remaining 5-10 years (1991-2000) as
246 the validation period. In the CONUS, the calibration period is chosen as 1980-2000, and the
247 validation period is from 2001 to 2014. When we know mean annual Q_s , Q_b , Q , P and W of the
248 first period, the parameters, i.e., W_p , V_p and U_p , can be derived from Eq. (14). Postulating the
249 parameters remain unchanged during two periods, we consequently can estimate the mean annual
250 Q_s , Q_b and Q of the second period using Eq. (14). Note that the catchment wetting W is calculated
251 as the difference of the P and estimated Q_s .

252 The surface flow fraction (*SFC*, the ratio of surface flow to precipitation) and baseflow fraction
253 (*BFC*, the ratio between baseflow and precipitation) represent the proportion of rainfall becoming
254 different runoff components, which are commonly used to quantify surface flow and baseflow
255 (Wang and Wu, 2013). Therefore, we evaluate the simulation of *SFC* and *BFC* as well as the
256 volume of runoff components.

257 The performance of the MPS model is evaluated by the coefficient of determination (R^2) and
 258 the root mean square error (RMSE):

$$R^2 = \left(\frac{\sum_{i=1}^N (X_{sim,i} - \bar{X}_{sim})(X_{obs,i} - \bar{X}_{obs})}{\sqrt{\sum_{i=1}^N (X_{sim,i} - \bar{X}_{sim})^2 \sum_{i=1}^N (X_{obs,i} - \bar{X}_{obs})^2}} \right)^2 \quad (15)$$

$$RMSE = \sqrt{\frac{1}{N} \sum_{i=1}^N (X_{sim,i} - X_{obs,i})^2} \quad (16)$$

259 where X represents the evaluated variable, i.e., mean annual Q , Q_s and Q_b , SFC and BFC in this
 260 study. The subscript obs and sim represents the observed and simulated value, respectively.
 261 Higher R^2 and lower RMSE indicate good model performance.

262 3.3. Attribution analysis

263 We split the data into the first period (1960-1990 in China and 1980-2000 in the CONUS) and
 264 the second period (1991-2000 in China and 2001-2014 in the CONUS) to attribute runoff
 265 components variation between two periods. Note that the attribution of ΔQ is only conducted in
 266 China because the E_0 in CAMELS dataset is a constant in each catchment. In the MPS model, we
 267 consider that the runoff changes between two long-term periods are caused by available water and
 268 other environmental and anthropogenic factors (such as land cover/use change and
 269 evapotranspiration variation) encoded by parameters. For the changes of surface flow (ΔQ_s) and
 270 total runoff (ΔQ), postulating that each variable is independent in the MPS model, the first-order
 271 approximation of the ΔQ_s and ΔQ from the second period to the first period can be expressed as
 272 (Milly and Dunne, 2002):

$$\Delta Q_s = \frac{\partial Q_s}{\partial P} \Delta P + \frac{\partial Q_s}{\partial W_p} \Delta W_p \quad (17a)$$

$$\Delta Q = \frac{\partial Q}{\partial P} \Delta P + \frac{\partial Q}{\partial U_p} \Delta U_p \quad (17b)$$

273 where the two terms on the right side of equation (17a) respectively represent changes in Q_s
 274 caused by changes in P (ΔQ_{s-P}) and other factors (ΔQ_{s-W_p}), and the two terms on the right side
 275 of equation (17b) respectively represent changes in Q caused by changes in P (ΔQ_P) and other
 276 factors (ΔQ_{W_p}). For convenience, we refer partial derivative coefficient $\frac{\partial Q_s}{\partial P}$, $\frac{\partial Q_s}{\partial W_p}$, $\frac{\partial Q}{\partial P}$ and $\frac{\partial Q}{\partial U_p}$ in

277 equation (17) as ζ_{Qs-P} , ζ_{Qs-Wp} , ζ_{Q-P} and ζ_{Q-Wp} , which can be calculated as:

$$\zeta_{Qs-P} = \frac{P^2 + 2PW_p}{(P + W_p)^2} \quad (18a)$$

$$\zeta_{Qs-Wp} = \frac{-P^2}{(P + W_p)^2} \quad (18b)$$

$$\zeta_{Q-P} = \frac{P^2 + 2PU_p}{(P + U_p)^2} \quad (18c)$$

$$\zeta_{Q-Wp} = \frac{-P^2}{(P + U_p)^2} \quad (18d)$$

278 The changes of baseflow (ΔQ_b) is induced by the variations of the W and V_p . However, we
279 focus more on the impact of P in application. Therefore, we combine equation (10), (11) and $W =$
280 $P - Q_s$, so the Q_b can be calculated as :

$$Q_b = \frac{P^2 W_p^2}{(P + W_p)(PW_p + PV_p + W_p V_p)} \quad (19)$$

281 The ΔQ_b can be attributed as the variations of P , W_p and V_p :

$$\Delta Q_b = \frac{\partial Q_b}{\partial P} \Delta P + \frac{\partial Q_b}{\partial W_p} \Delta W_p + \frac{\partial Q_b}{\partial V_p} \Delta V_p \quad (20)$$

282 where the three terms on the right side of equation (20) respectively represent changes in Q_b
283 caused by changes in P (ΔQ_{b-P}), W_p (ΔQ_{b-Wp}) and V_p (ΔQ_{b-Vp}). The partial derivative
284 coefficient $\frac{\partial Q_b}{\partial P}$ (ζ_{Qb-P}), $\frac{\partial Q_b}{\partial W_p}$ (ζ_{Qb-Wp}) and $\frac{\partial Q_b}{\partial V_p}$ (ζ_{Qb-Vp}) can be calculated as:

$$\zeta_{Qb-P} = \frac{2P^2 W_p^3 V_p + P^2 W_p^4 + 2P W_p^4 V_p}{(P + W_p)^2 (PW_p + PV_p + W_p V_p)^2} \quad (21a)$$

$$\zeta_{Qb-Wp} = \frac{P^4 W_p^2 + 2P^4 W_p V_p + 2P^3 W_p^2 V_p}{(P + W_p)^2 (PW_p + PV_p + W_p V_p)^2} \quad (21b)$$

$$\zeta_{Qb-Vp} = \frac{-P^2 W_p^2}{(P + W_p)^2 (PW_p + PV_p + W_p V_p)^2} \quad (21c)$$

285 To verify the applicability of the MPS model for runoff components attribution, we compare
286 the calculated ΔQ_s , ΔQ_b and ΔQ using equation (17) and (20) with the observed ΔQ_s , ΔQ_b
287 and ΔQ between two periods. The evaluation metrics are R^2 and RMSE.

288 The relative contribution ratios of P and other factors to runoff components change are
289 calculated as:

$$\eta_P = \frac{|\Delta Q_{y-P}|}{|\Delta Q_{y-P}| + |\Delta Q_{y-Wp}| + |\Delta Q_{y-Vp}|} \times 100\% \quad (22a)$$

$$\eta_{Wp} = \frac{|\Delta Q_{y-Wp}|}{|\Delta Q_{y-P}| + |\Delta Q_{y-Wp}| + |\Delta Q_{y-Vp}|} \times 100\% \quad (22b)$$

$$\eta_{Vp} = \frac{|\Delta Q_{y-Vp}|}{|\Delta Q_{y-P}| + |\Delta Q_{y-Wp}| + |\Delta Q_{y-Vp}|} \times 100\% \quad (22c)$$

290 where η_P , η_{Wp} and η_{Vp} are the relative contribution ratios of P , W_p and V_p to runoff
291 components, respectively. We subsequently use the absolute values of η to identify the dominant
292 factor impacting runoff components.

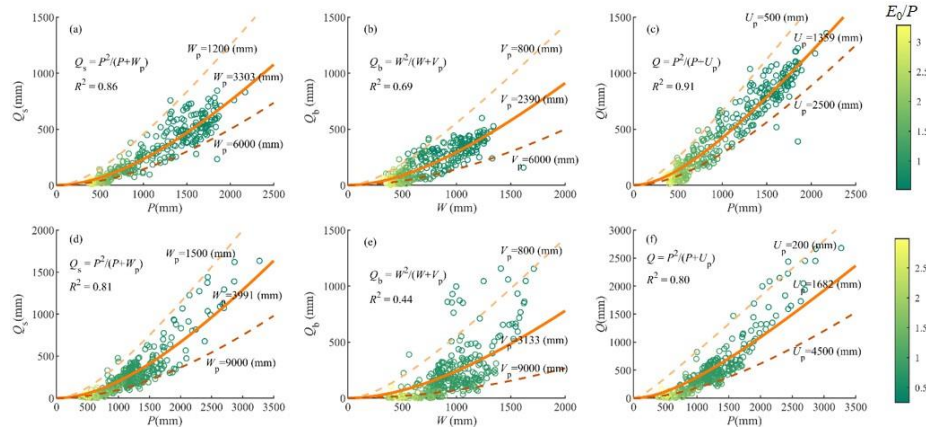
293 4. Results

294 4.1. Inter-Catchment Variability of Runoff Components

295 We employ the MPS model to fit the relationship between mean annual available water and
296 runoff components. In China, as shown in Figure 4(a-c), the MPS model performs well in
297 describing runoff components variability between catchments, with R^2 values of 0.86, 0.68 and
298 0.91 for fitting Q_s , Q_b and Q , respectively. The solid lines are the best-fitted MPS curves derived
299 using the least squares fitting algorithm, implying the median values of different parameters. We
300 also give the potential upper and lower limits of W_p , V_p and U_p across catchments. Similarly,
301 Figure 4(d-f) illustrates that the MPS model achieves good fitting in the CONUS, with R^2 of 0.81,
302 0.44 and 0.80 for fitting Q_s , Q_b and Q , respectively. The fitted parameters in the CONUS are
303 smaller than those in China, while they have more comprehensive ranges between catchments,
304 meaning a more significant heterogeneity in climate and underlying surface.

305 Figures 4 demonstrates that the MPS model can effectively reproduce the spatial variability of
306 different runoff components along with the aridity index (E_0/P), which are primarily controlled by
307 the available water of the corresponding partition stage. The performance of MPS model to fit Q_s
308 and Q is better than that of Q_b , indicating that the factors controlling Q_b are more complicated and

309 not fully reflected in the model. With catchment properties and other factors (integrated by the
 310 parameters in the MPS model) remaining unchanged, the more the available water, the higher the
 311 runoff generated. Conversely, smaller parameter values are associated with greater runoff for a
 312 given amount of available water.



313 **Figure 4.** The MPS model relating (a) P versus Q_s , (b) W versus Q_b and (c) P versus Q in China
 314 and (d) P versus Q_s , (e) W versus Q_b and (f) P versus Q in the CONUS. The lines are the fitted
 315 MPS curves with best fitting (solid line) and potential upper limit and lower limit (dashed lines)
 316 parameters.

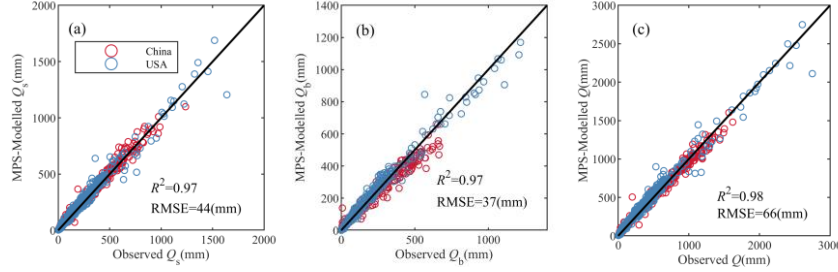
318 4.2. Validation of Runoff Components Estimation

319 Figure 5 shows the estimated mean annual Q_s , Q_b and Q in validation periods using the MPS
 320 model with inverted parameters in equation (14) in China and the CONUS. The simulated runoff
 321 components match very well with the observed, with R^2 greater than 0.97 and RMSE less than 66
 322 mm. There is no significant difference in the performance in simulating Q_s , Q_b , and Q , except for
 323 a slight underestimation in simulating Q_b of catchments in China and some in the CONUS.

324 In panels (a), (b), and (c), we observe that the scatter points for both China (red circles) and the
 325 CONUS (blue circles) are closely aligned with the 1:1 line, further underscoring the strong
 326 correlation between modeled and observed values. Specifically, the results show that the MPS
 327 model effectively captures surface flow (Q_s), baseflow (Q_b), and total runoff (Q) for both regions.
 328 Despite the generally good performance, a slight underestimation of Q_b is evident in a subset of
 329 catchments in China and, to a lesser extent, in the CONUS. However, these discrepancies are

330 minimal and do not significantly detract from the model's overall accuracy.

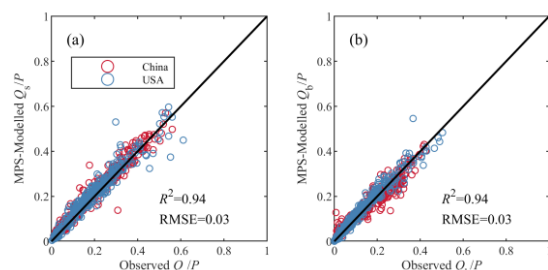
331



332 **Figure 5.** The observed and simulated mean annual (a) surface flow, (b) baseflow and (c) total
333 runoff by the MPS model in China (red circles) and the CONUS (blue circles).

334 Figure 6 presents the estimation of *SFC* and *BFC* in validation periods using the MPS model.
335 Similar to the simulation of Q_s , the two methods also show highly consistent estimation of *SFC*
336 (panel (a)), with R^2 of 0.94 and RMSE of 0.03. This demonstrates the MPS model's robust
337 capability to estimate the surface flow fraction in China and the CONUS, closely aligning with
338 the observed data. Panel (b) presents the estimation of *BFC*, where the MPS model achieves
339 significant accuracy, reflected by the same R^2 and RMSE values (0.94 and 0.03, respectively).
340 This strong performance indicates that the MPS model is highly effective in simulating *SFC* and
341 *BFC* across various catchments.

342

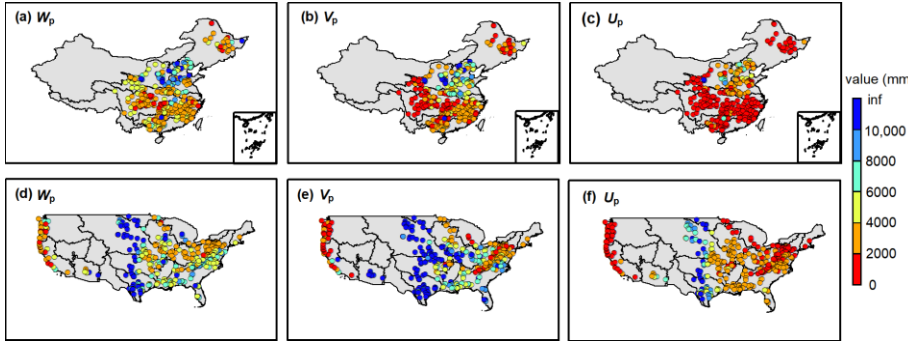


343 **Figure 6.** The observed and simulated (a) surface flow fraction (Q_s/P) and (b) baseflow fraction
344 (Q_b/P) by the MPS model in China (red circles) and the CONUS (blue circles).

345 Figure 5 and Figure 6 document that the MPS model can effectively estimate the multi-year
346 average of all runoff components and the proportions of precipitation allocated to runoff.
347 The good validation performance of the MPS model verified our hypothesis that the parameters

348 in the general formulations remain stable at the mean annual time scale. The parameters reflect
349 the comprehensive impact of climate and catchment characteristics, i.e., catchment wetting
350 potential (W_p), vaporization potential (V_p) and the upper limit of the portion remaining after
351 precipitation is allocated to runoff (U_p). As shown in Figure 7(a-c), the spatial distribution of the
352 parameters across China exhibits pronounced divergence between the northern and southern
353 catchments, as well as the eastern and the western. The W_p , V_p and U_p exhibit similar spatial
354 patterns, which can be approximately divided into two tiers from north to south. In the catchments
355 of the Songliao River Basin in the northeast, the Yangtze River Basin and Pearl River Basins in
356 the south, the parameters are relatively small, with W_p and U_p ranging from 0 to 2000 mm, and V_p
357 from 0 to 4000 mm, resulting large flow. In the catchments of the Yellow River Basin, Huaihe
358 River Basin and Haihe River Basin in the north, the parameters are quite large and usually more
359 than 5000 mm and even 8000 mm, leading to small flow. From west to east, W_p exhibits higher
360 values in the Yangtze and Yellow Rivers Basin sources, whereas V_p and U_p are smaller in the
361 source regions. This disparity may reflect variations in the two-stage partition of precipitation,
362 contributing to spatial differences in total runoff. According to Figure 7(c), we can deduce that
363 the spatial distribution of higher total runoff in south and lower in north across China, aligning
364 with previous observational studies (He et al., 2021; He et al., 2022; Yang et al., 2019).

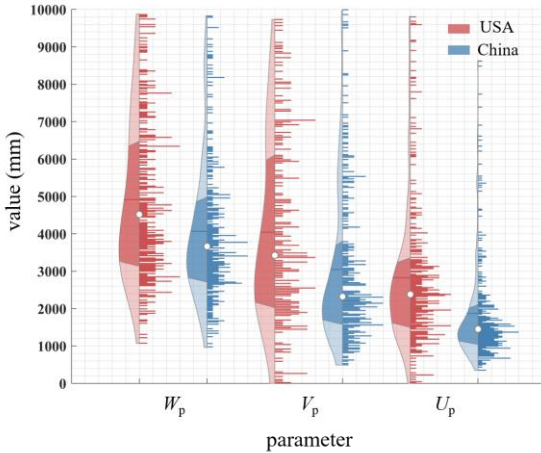
365 Figure 7(d-f) shows an evident west-east discrepancy of the three parameters across the
366 CONUS. Typically, W_p , V_p and U_p of the catchments in the west coast and eastern regions are less
367 than 5000 mm, while parameters in the central United States are extensive with values more than
368 8000 mm. This indicates relatively low flow in the central regions. Notably, the parameters upper
369 limits in the catchments of the CONUS are significantly higher than those in China. The
370 extremely large values may be associated with significant parameter uncertainty (Gnann et al.,
371 2019). Figure 7 demonstrates that the values of the three parameters are larger in arid catchments
372 and their spatial patterns are similar to that of climate zoning, which provides insights for
373 parameterization.



374 **Figure 7.** The (a) wetting potential (W_p), (b) vaporization potential (V_p) and (c)

375 evapotranspiration potential (U_p) of the catchments in China and (d) wetting potential (W_p), (e)
 376 vaporization potential (V_p) and (f) evapotranspiration potential (U_p) of the catchments in the
 377 CONUS.

378 Figure 8 shows the violin plots of the parameters in the catchments of China and the CONUS.
 379 The median values of W_p , V_p , and U_p in China are 3659 mm, 2220 mm and 1453 mm,
 380 respectively. The median values of W_p , V_p , and U_p in the CONUS are 4531 mm, 3424 mm and
 381 2385 mm, respectively. Overall parameters in China are smaller and denser than those in the
 382 CONUS, implying a smaller variability of runoff components in China. Furthermore, the C_v value
 383 of V_p (1.6 in China and 6.8 in the CONUS) is the largest, followed by U_p (0.9 in China and 1.6 in
 384 the CONUS), and the smallest for W_p (0.6 in China and 1.5 in the CONUS). This indicates that
 385 the parameter dispersion controlling the second partition stage of rainfall is the greatest, which
 386 could partly account for the challenges in accurately estimating Q_b .

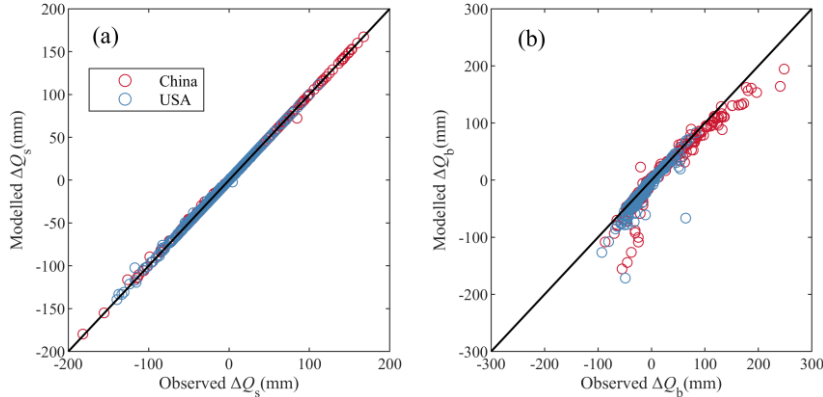


388

389 **Figure 8.** Violin plots of the parameters in the catchments of China and the CONUS. In each
 390 violin plot, the left side represents the distribution, with the shaded area indicating the box plot,
 391 the dot representing the mean, and the right side showing the histogram. The length of the
 392 histogram represents the number of catchments (values larger than 10,000 are not shown).

393 4.3. The Changes Attribution of Runoff Components

394 The metrics to evaluate the attribution results between the changes of the observed and
 395 simulated runoff components are shown in Table 2. We use the MPS model to estimate the
 396 changes of Q_s (ΔQ_s), Q_b (ΔQ_b) and Q (ΔQ) from two long-term periods by equation (17) and
 397 (20), and for comparison, we use the Budyko framework to estimate ΔQ , which is considered as
 398 the changes induced by P , E_0 , and parameter n (the calculation formulations can refer Zhang et al.
 399 (2018)). The estimated and observed runoff components variations exhibit high consistency
 400 (Figure 9), with an R^2 of 0.99 and RMSE of 1.6 mm of ΔQ_s attribution and R^2 of 0.88 and RMSE
 401 of 18 mm of ΔQ_b attribution, respectively. As for ΔQ attribution, both the MPS model and the
 402 Budyko framework can attain satisfactory performance, while the MPS model has a higher R^2
 403 (0.91) than the Budyko framework (0.89). Table 2 demonstrates that the MPS model can
 404 accurately quantify changes in runoff components over two periods. Subsequently, we quantify
 405 the contribution of precipitation and other factors (encoded by parameter W_p and V_p) to ΔQ_s and
 406 ΔQ_b .



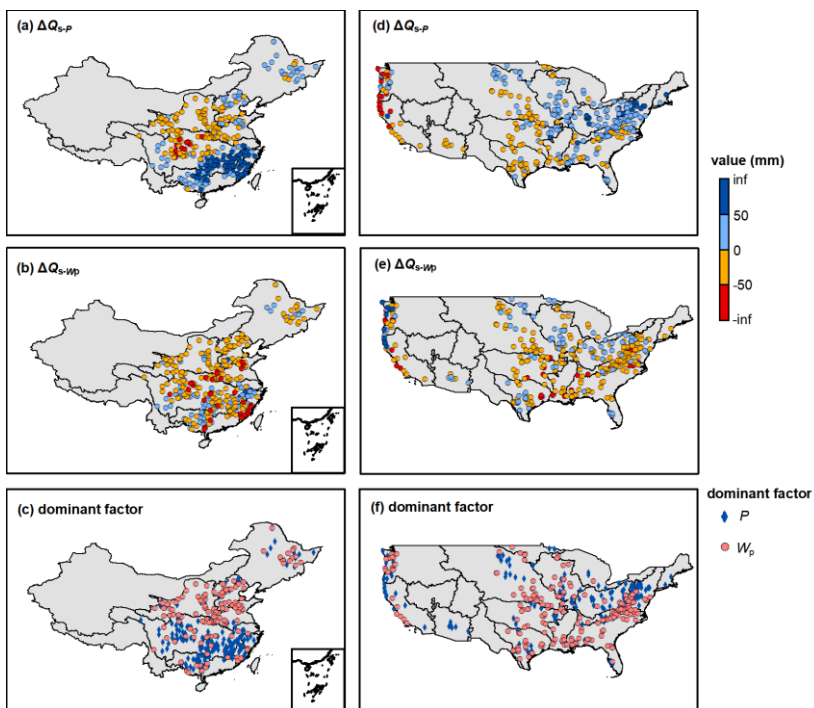
407 **Figure 9.** The observed and modelled (a) surface flow and (b) baseflow by the MPS model.

408 **Table 2.** The metrics of the attribution validation

Variables	R^2	RMSE (mm)
ΔQ_s	0.99	1.6
ΔQ_b	0.90	16
ΔQ (the MPS model)	0.91	42
ΔQ (the Budyko framework)	0.89	41

410 Figure 10 shows the ΔQ_s induced by P (ΔQ_{s-P}) and other factors (ΔQ_{s-W_p}) along with the
 411 dominant factor in the catchments of China and the CONUS. From 1960-1990 to 1991-2000 in
 412 China, the multi-year variation in P has resulted in Q_s change ranging from -105 to 344 mm,
 413 mainly increasing Q_s in the catchments of the Songliao River Basin, the middle and lower
 414 Yangtze River Basin, the Southeast River Basin and Pearl River Basin, and decreasing Q_s in the
 415 catchments of the Yellow River Basin and the upper Yangtze River Basin (Figure 10(a)). The
 416 variations of other factors, such as land use/cover change and human activities, have resulted in
 417 Q_s change ranging from -186 to 124 mm, primarily decreases Q_s in 70% catchments (Figure
 418 10(b)). P and other W_p are the dominant factor altering Q_s in southern and northern China,
 419 respectively (Figure 10(c)). From 1980-2000 to 2000-2014 in the CONUS, variation in P has
 420 resulted in Q_s change ranging from -469 to 149 mm, mainly increasing Q_s in the catchments of
 421 Interior Plains (except Great Plains), Coastal Plain, Interior highlands and Appalachian Plain, and
 422 decreasing Q_s in the catchments of the Great Plains and Pacific Mountains (the physiographic

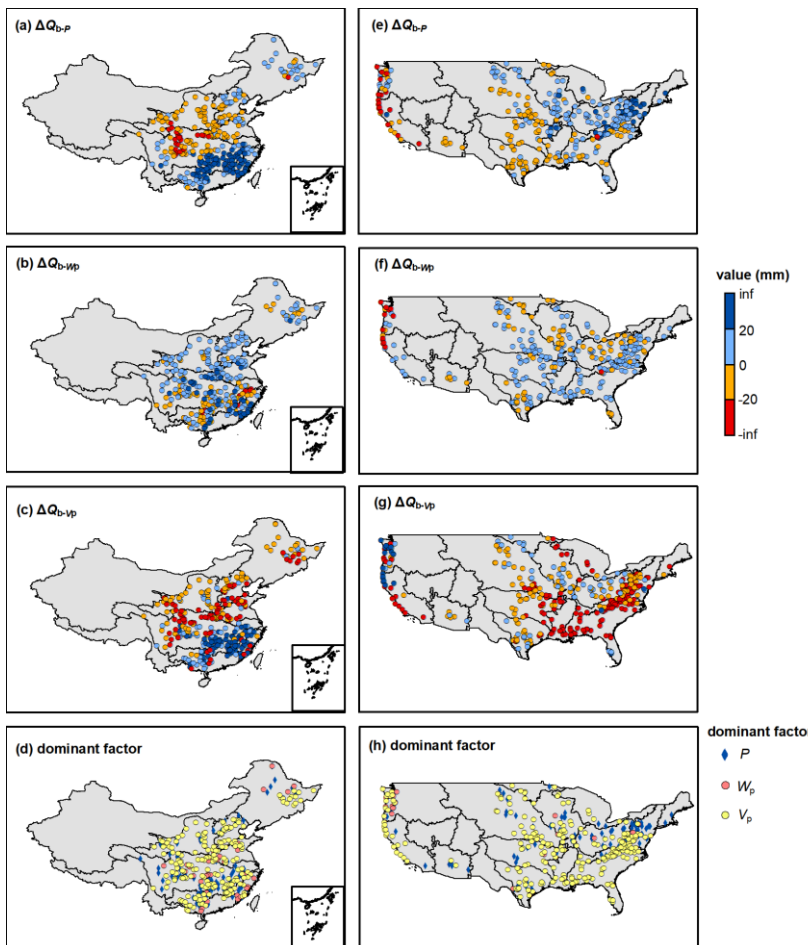
423 divisions are referred to Wu et al. (2021)) (Figure 10(d)). The variations of other factors have
 424 resulted in Q_s change ranging from -230 to 467 mm, primarily decreases Q_s in 75% catchments
 425 (Figure 10(e)). The catchments in the CONUS dominated by P and W_p account for 43% and 57%,
 426 respectively (Figure 10(f)).



427
 428 **Figure 10.** The surface flow change induced by precipitation and wetting potential (W_p) along
 429 with the dominant controlling factor.

430 Figure 11 shows the ΔQ_b induced by P (ΔQ_{b-P}), W_p (ΔQ_{b-Wp}) and V_p (ΔQ_{b-Vp}) in the
 431 catchments of China and the CONUS. The spatial pattern of the effect of P on Q_b is similar to that
 432 of the Q_s , resulting in Q_b change from -38 to 79 mm in China (Figure 11(a)) and -129 to 92 mm in
 433 the CONUS (Figure 11(e)), respectively. Catchment wetting potential has a positive effect on Q_b
 434 in 70% and 75% catchments of China and the CONUS, respectively (Figure 11(b) and (f)), mainly
 435 in the northern China and the Interior Highlands, Coastal Plain and Appalachian Highlands of the
 436 CONUS. Vaporization potential has a negative effect on Q_b in 56% and 77% catchments of China
 437 and the CONUS, respectively, mainly in the upper Yangze River Basin and northern China and

438 the central and southeastern CONUS (Figure 11(c)and (g)). Although V_p is the dominant factor
 439 controlling Q_b variation in most catchments in both China (62%) and the CONUS (71%) (Figure
 440 11(d)and (h)), the contributions of the P , W_p and V_p are not significantly discrepant in terms of
 441 magnitude.



442
 443 **Figure 11.** The baseflow change induced by precipitation, wetting potential (W_p) and
 444 vaporization potential (V_p) along with the dominant controlling factor.

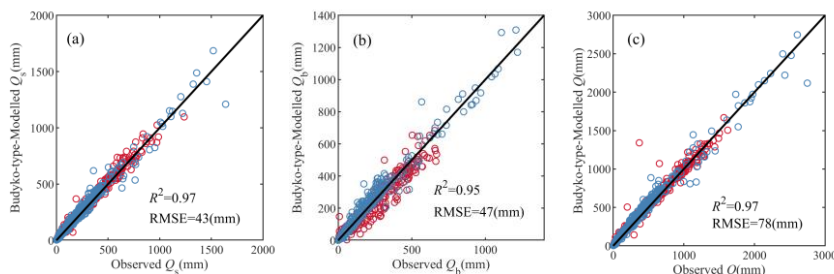
445 Overall, Figure 10 and 11 illustrate that the variation of Q_s is jointly controlled by P and other
 446 factors, while the variation of Q_b is mainly influenced by V_p . This demonstrates that Q_s is closely
 447 related to rainfall and soil storage capacity, while Q_b is more affected by catchment attributes,

448 atmospheric water and energy demand, etc. In regions where runoff components are reduced,
 449 focus should be given to the risks of drought and river discontinuity; conversely, in areas
 450 experiencing runoff components increase, there is a need to guard against the risk of flooding.

451 **5. Discussion**

452 **5.1. Superiorities of the MPS Model**

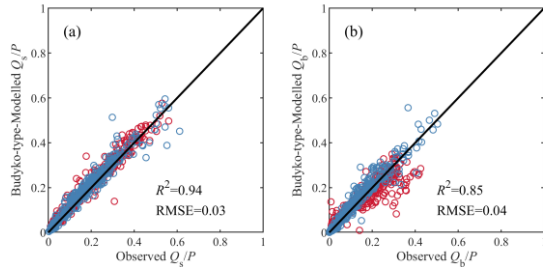
453 The researches about long-term runoff components quantification and attribution are currently
 454 fragmented and region-specific (Beck et al., 2013; Gnann, 2021). This study has developed a
 455 general formulation (the MPS model) through observational data analysis and theoretical
 456 derivation based on the Ponce-Shetty model, unveiling the patterns of variability in different
 457 runoff components at mean annual time scale. Compared to the commonly used Budyko-type
 458 formulations, it can not only estimate mean annual Q and Q_b , but also can depict the variability of
 459 Q_s . Figure 12 shows the estimated mean annual runoff components by the Budyko-type
 460 formulations (equations in the second and fifth rows of Table 1 in this paper). The Budyko-type
 461 formulations also achieve good validation performance, with R^2 greater than 0.95 and RMSE less
 462 than 78 mm. Although the MPS model and the Budyko-type formulations are comparable in
 463 terms of R^2 , especially with almost equal simulation results of Q_s , the MPS model reduced the
 464 RMSE values by 10 mm and 12 mm for estimating Q_b , respectively.



465
 466 **Figure 12.** The observed and simulated mean annual (a) surface flow, (b) baseflow and (c) total
 467 runoff by the Budyko-type formulations in China (red circles) and the CONUS (blue circles).

468 Figure 13 presents the estimation of SFC and BFC in validation periods using the Budyko-type
 469 formulations. The two methods also show highly consistent estimation of SFC , with R^2 of 0.94

470 and RMSE of 0.03. However, the Budyko-type formulations underestimate the *BFC* of most
 471 catchments in China, while the MPS model greatly improves the simulation accuracy of *BFC*.



472

473 **Figure 13.** The observed and simulated (a) surface flow fraction (Q_s/P) and (b) baseflow fraction
 474 (Q_b/P) by the MPS model in China (red circles) and the CONUS (blue circles).

475 In conclusion, the MPS model has comparable capability in simulating Q_s and *SFC* to that of
 476 Budyko-type formulations. Moreover, it outperforms Budyko-type formulations in estimating Q_b
 477 and Q , and reveals superiority in estimating *BFC*. By characterizing runoff components as
 478 functions of available water at corresponding stages with a composite parameter, the MPS model
 479 is more concise in form and eliminates additional and complex parameter computations, thereby
 480 facilitating broader application in large-sample investigations.

481 In addition to precisely quantifying runoff components and the allocation of precipitation, this
 482 model has innovatively attributed the contributions of different factors on the changes of Q_s and
 483 Q_b . Our results show that the variation of Q_s is jointly controlled by P and other factors. P plays
 484 an dominant role in the variation of Q_s in the catchments of the Yangtze River Basin, Southeast
 485 Basin and Pearl River Basin of China and the west coast of the CONUS, where precipitation has
 486 been reported to have undergone significant changes (Li et al., 2021; Mallakpour and Villarini,
 487 2017; Massoud et al., 2020; Xu et al., 2022). This is possibly due to more extreme precipitation
 488 events and summer rainfall in the middle-lower Yangtze River Basin (Ye et al., 2018) and an
 489 increasing trend in the frequency of heavy precipitation over large areas of the CONUS
 490 (Mallakpour and Villarini, 2017). Previous studies reported that the variation of Q in these
 491 regions are dominated by P (He et al., 2022; Huang et al., 2016). Now it seems that P mainly
 492 affects the first allocation stage (Q_s) and consequently change total runoff. The variation of Q_b is
 493 mainly influenced by V_p , indicating that we should pay more attention to the changes of

494 catchment attributes, atmospheric water and energy demand in most catchments when
495 investigating Q_b .

496 Overall, this conceptual model extracted from observed rainfall-runoff data provides a concise,
497 general and effective tool for predicting runoff components, and evaluating their responses to
498 climate and environment under global change.

499 **5.2. Parameter Interpretation**

500 In the MPS model, each runoff component is associated with a parameter that can be
501 interpreted as the upper limit of the remaining portion of available water after it has been
502 partitioned into runoff at each stage. For instance, in the first stage, precipitation is allocated to
503 surface flow and catchment wetting, with W_p representing the upper limit of catchment wetting,
504 which describes the catchment's storage capacity related to soil, topography and so on (Cheng et
505 al., 2023). W_p is influenced by soil properties and available storage capacity, determining the
506 fraction of precipitation that rapidly becomes surface runoff versus what is stored. For the second
507 stage, the available water comes from catchment wetting, which is then allocated to baseflow and
508 vaporization. The parameter V_p is the upper limit of the fraction of wetting returned to the
509 atmosphere as water vapor (Ponce and Shetty, 1995), and is likely responds to subsurface
510 characteristics such as aquifer permeability and geological layering. For instance, in highly
511 heterogeneous aquifers with well-developed preferential pathways (e.g., fractured rock or karst
512 systems), water is rapidly drained toward the stream, leading to a higher efficiency of baseflow
513 production and thus a lower V_p value (as less water is retained for evaporation). Conversely, in
514 catchments with more homogeneous, porous media (e.g., sandy aquifers), water movement is
515 slower and more diffuse, potentially allowing for a greater fraction of stored water to be
516 evaporated, resulting in a higher V_p . For the total runoff, we consider precipitation as the available
517 water competing with evapotranspiration, whose upper limit is represented by the parameter U_p .
518 Similar to V_p in the second stage, U_p can be regarded as a sort of atmospheric water and energy
519 limit (somewhat analogous to potential evapotranspiration) and emerges from the interaction of
520 the available energy, vegetation and other catchment characteristics. To some extent, the MPS
521 model links Q_s and Q_b with Q using P in the first trade-off and V_p in the second trade-off, so that
522 the forms of different runoff components can be unified.

带格式的: 字体: (默认) Times New Roman, (中文) 宋体, 小四, 字体颜色: 黑色

带格式的: 字体: (默认) Times New Roman, (中文) 宋体, 小四, 字体颜色: 黑色

523 Additionally, we compared the distribution of the parameters in the MPS model with that in
524 Gnann (Gnann et al., 2019) and Siva's work (Sivapalan et al., 2011), which did not omit the
525 initial abstraction coefficients λ_s and λ_b . There is a very similar spatial pattern of W_p and V_p in
526 the CONUS. Specifically, high W_p can be seen in the middle of the United States (Great Plains)
527 and the east (southern parts of the Appalachians) (Figure 7(d)), and high V_p can be seen in the
528 middle of the United States (Great Plains) and all southern regions (Figure 7(e)). This, to some
529 extent, illustrates the rationality of the simplification of the original Ponce-Shetty model in
530 describing the spatial variability of runoff components. According to Ponce and Shetty (1995)
531 and Sivapalan et al. (2011), the products $\lambda_s W_p$ and $\lambda_b V_p$ are viewed as the initial abstraction to
532 generate runoff. This definition is reasonable for short-term scales, such as event and annual
533 scales. However, on the multi-annual scale, the catchment maintains a state of water balance and
534 water losses can be disregarded (Han et al., 2020). Hence, simplifying λ to zero is rational to
535 quantify and attribute runoff components and offer a new perspective on the long-term catchment
536 water balance.

537 5.3. Uncertainties and Future Improvements

538 It is important to acknowledge several uncertainties in this study. First, the definition of
539 "baseflow" itself introduces uncertainty. Although widely used as a collective term for delayed
540 streamflow components, baseflow encompasses contributions from hydrologically distinct
541 sources such as groundwater drainage, hyporeic exchange, snowmelt, and deeper subsurface
542 leakage-each with distinct origins, timescales, and sensitivities to environmental factors. For
543 instance, groundwater flow and deep leakage are strongly controlled by geological heterogeneity,
544 including the distribution of rock types, porosity, permeability, faults, and fractures (Schiavo et
545 al., 2023). In contrast, snowmelt baseflow, on the other hand, is mainly driven by temperature
546 variations within interannual to decadal climate cycles.

547 The definition of baseflow directly influences the selection of catchment areas. Guided by this
548 macro-scale definition-viewing baseflow as the relatively stable portion of total runoff-we
549 included large catchments in our analysis. While this inclusion may be a source of error, it does
550 not affect the key finding that the MPS model effectively captures the variability of mean annual
551 runoff components across catchments. A sensitivity analysis of the model's performance under

带格式的: 字体: (默认) Times New Roman, (中文) 宋体, 小四, 字体颜色: 黑色

带格式的: 字体: (默认) Times New Roman, (中文) 宋体, 小四, 字体颜色: 黑色

带格式的: 字体: (默认) Times New Roman, (中文) 宋体, 小四, 字体颜色: 黑色

带格式的: 字体: (默认) Times New Roman, (中文) 宋体, 小四, 字体颜色: 黑色

带格式的: 字体: (默认) Times New Roman, (中文) 宋体, 小四, 字体颜色: 黑色

带格式的: 字体: (默认) Times New Roman, (中文) 宋体, 小四, 字体颜色: 黑色

带格式的: 字体: (默认) Times New Roman, (中文) 宋体, 小四, 字体颜色: 黑色

552 different area thresholds is provided in Appendix Table A1. Future studies could combine isotope
553 tracing with hydrological modeling to better quantify the contributions of these different sources.
554 Second, methodological uncertainty arises from the digital filter method (i.e., the Lyne–Hollick
555 algorithm) for baseflow separation. While practical and widely applied, this approach is
556 deterministic and does not explicitly account for uncertainties related to aquifer heterogeneity,
557 such as spatial variability in hydraulic conductivity, preferential flow paths, or geologic structures.
558 Future work could adopt stochastic frameworks such as Monte Carlo simulation by generating
559 multiple realistic realizations of aquifer heterogeneity to obtain more robust and probabilistic
560 baseflow estimates (Schiavo et al., 2023). Additionally, our study did not take into account the
561 spatial heterogeneity of groundwater flow, particularly its preferential pathways through fractures,
562 macropores, or highly permeable sedimentary layers. Event-scale analyses indicate that
563 stormflow volumes and hysteresis patterns covary with subsurface connectivity and its timing.
564 For example, Zuecco et al. (2019) who used graph-theory metrics to quantify connectivity in
565 headwater catchments and linked maximum connectivity to stormflow. While our study operates
566 at mean-annual scales, these findings are consistent with our interpretation that geological
567 heterogeneity and preferential pathways (fractures, karst, macropores) modulate the V_p dispersion
568 and, in turn, the aggregate baseflow fraction. Future work could employ numerical models or
569 distributed hydrological models that explicitly represent geological structures to better capture the
570 effects of preferential flow paths at smaller scales.

571 The sensitivity of runoff to changes in climatic and environmental factors has always been
572 highly anticipated. Schaake (1990) first introduced the concept of climate elasticity coefficients to
573 quantify it, defined as the ratio of the relative change in mean annual runoff to the relative change
574 in climatic factors. Various expressions have been widely applied in evaluating the hydrological
575 response to multi-annual average climate change (Sun et al., 2014; Xu et al., 2014). The only
576 climatic factor in the MPS model is P , so we primarily focuses on the elasticity of runoff
577 components to P (ε), which can be expressed as $\varepsilon_{y-P} = \frac{\partial Q_y}{\partial P} / \frac{Q_y}{P}$, quantifying the percentage of
578 runoff components change caused by 1% change in P .

579 Figure 14 shows elasticities of Q , Q_s and Q_b to P derived from the MPS model in the CONUS.
580 We compare the elasticity distribution of the work conducted by Harman et al. (2011), who did

带格式的: 字体: (默认) Times New Roman, (中文) 宋体, 小四, 字体颜色: 黑色

带格式的: 字体: (默认) Times New Roman, (中文) 宋体, 小四, 字体颜色: 黑色

带格式的: 字体: (默认) Times New Roman, (中文) 宋体, 小四, 字体颜色: 黑色

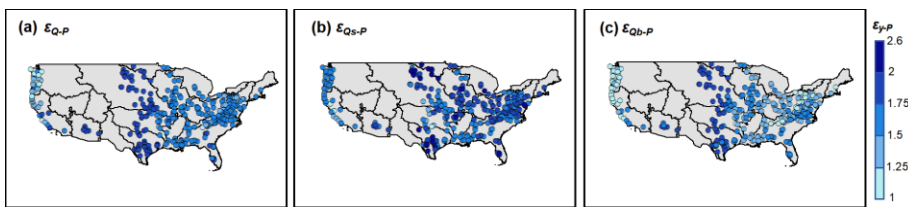
带格式的: 字体: (默认) Times New Roman, (中文) 宋体, 小四, 字体颜色: 黑色

带格式的: 字体: (默认) Times New Roman, (中文) 宋体, 小四, 字体颜色: 黑色

带格式的: 字体: (默认) Times New Roman, (中文) 宋体, 小四, 字体颜色: 黑色

带格式的: 字体: (默认) Times New Roman, (中文) 宋体, 小四, 字体颜色: 黑色

581 not omit the initial abstraction coefficients λ . In humid catchments with the aridity index of less
 582 than 1 (such as the west coast and eastern regions of the CONUS), the results from both studies
 583 are very close, with elasticity values from 1 to 2. However, the MPS model noticeably
 584 underestimates the runoff sensitivity to P in semi-arid and arid catchments (such as the Great
 585 Plains). This may be due to the error caused by the assumption that λ is a constant when deriving
 586 the MPS model.



587 **Figure 14.** The elasticity of (a) total runoff, (b) surface flow and (c) baseflow to precipitation
 588 derived the MPS model.

589 Additionally, the secondary rainfall processes, such as initial abstraction to generate runoff,
 590 precipitation intensity and seasonality should be considered in these regions, which have been
 591 proven to have a significant impact in attribution analysis (He et al., 2022; Ning et al., 2022;
 592 Zhang, 2015). Moreover, the potential evapotranspiration (E_0), which indicates the impact of
 593 energy constraints (Huang et al., 2019; Wu et al., 2020), is quite significant in arid and semi-arid
 594 catchments and should be taken into account.

595 In this paper, we interpret the parameters (i.e., W_p , V_p and U_p) as a potential upper limit of each
 596 partition stage competing with corresponding runoff components following the annual
 597 Ponce-Shetty model. It is intriguing to discuss whether the connotation of the parameters has
 598 changed from annual to mean annual time scale. On a long-term scale, the initial abstraction
 599 coefficient (i.e., λ_p and λ_w) can be simplified as zero, indicating the loss for generating runoff is
 600 negligible. However, to what extent the initial abstraction coefficient affect precipitation partition
 601 at shorter time scales is still under-determined. The physical and theoretical interpretation of
 602 parameters and their impacts at different time scales are temporarily outside the scope of this
 603 study. However, it is valuable to further research in future work. In addition, the seasonality of
 604 rainfall measures the concentration of precipitation within a year. The more concentrated the
 605 precipitation, the more likely it is to generate surface runoff, resulting in greater intra-annual

607 fluctuations in the BFI and a lower annual BFI. In contrast, in catchments with evenly distributed
608 precipitation, soil water and groundwater are replenished consistently and gradually, leading to
609 relatively stable intra-annual BFI and a higher annual BFI.

610 The MPS model has only one parameter for controlling each runoff component, which is
611 arguably simplified but dependent on calibration, and their physical meaning needs further
612 explanation. We still need to explain the parameters in terms of regional patterns of climatic
613 and/or catchment attributes, meaning that currently this model can only be applied to gauged
614 catchments with runoff observations and challenging to transfer to ungauged basins. Cheng et al.
615 (2022) proposed two machine learning methods to characterize the parameter of the Budyko
616 framework and further employed them in estimating global runoff partition (Cheng et al., 2023).
617 Results show that parameters related to vegetation (such as root zone storage capacity, water use
618 efficiency and vegetation coverage) and climate (such as precipitation depth and climate
619 seasonality) are the primary controlling factors of the parameter. Similar work can be referred to
620 (Chen and Ruan, 2023). These investigations provide priori knowledge for quantitatively linking
621 the parameters of the MPS model to climate forcing and catchment attributes in future work.

622 **6. Conclusion**

623 We developed a general formulation (the MPS model) to estimate mean annual runoff
624 components as a function of available water with a synthetic parameter based on a two-stage
625 partition theory, and validated it over 662 catchments across China and the CONUS with further
626 attribution analysis. The concise MPS model provides more accurate runoff components
627 estimation and innovative attribution, offering new insights to long-term water balance and giving
628 additional superiorities toward making predictions of runoff variation under global change. The
629 main conclusions are as follows:

630 (1) The investigated catchments fit well with the MPS model, with R^2 of 0.86, 0.68 and 0.91 for
631 fitting Q_s , Q_b and Q in China and R^2 of 0.81, 0.44 and 0.80 for fitting Q_s , Q_b and Q in the CONUS,
632 implying the MPS model can well reproduce the spatial variability of different runoff
633 components.

634 (2) The MPS model effectively simulates multi-year runoff components with R^2 exceeding 0.97,

635 and the proportion of runoff components relative to precipitation with R^2 exceeding 0.94. The
636 spatial distribution of the parameters across China and the CONUS is related to that of climate
637 zoning.

638 (3) The MPS model has proved effective in quantifying the variations of runoff components
639 induced by precipitation and environmental factors. The estimated and observed ΔQ_s , ΔQ_b and
640 ΔQ exhibit high consistency, with an R^2 of 0.99 and RMSE of 1.6 mm of ΔQ_s attribution, R^2 of
641 0.90 and RMSE of 16 mm of ΔQ_b attribution and R^2 of 0.91 and RMSE of 42 mm of ΔQ
642 attribution, respectively. The variation of Q_s is jointly controlled by P and environmental factors,
643 while the variation of Q_b is mainly influenced by V_p in most catchments.

644 In general, this study proposes a general formulation for effectively estimating and attributing
645 the mean annual runoff, surface flow and baseflow. The structure is simple with few parameters
646 and clear physical significance. Its reliability has been authenticated, providing new insights for
647 analyzing watershed water resources in changing environments.

648

649 **Author Contribution**

650 Y.H: conceptualization; model development/theoretical derivation; investigation; calculation;
651 formal analysis; visualization; writing original draft.
652 H.Y: conceptualization; model development/theoretical derivation; data curation; writing review
653 & editing; supervision; funding acquisition.
654 C.L.: conceptualization; data analysis; visualization; writing review & editing
655 Y.H. conceived and
656 designed the study, collected and analyzed the data, and wrote the manuscript. C.L. participated in
657 the study design, provided intellectual insights, and reviewed the manuscript for important
658 intellectual content. C.L. and H.Y. guided the research process and critically reviewed the
659 manuscript. All authors have read and approved the final version of the manuscript.

659 **Competing interests**

660 The authors declare that they have no conflict of interest.

661 _____

带格式的: 正文, 行距: 单倍行距

662 **Appendix**

663 Table A1 The coefficient of determination (R^2) and model parameters for the MPS curve fittings under different
664 area thresholds for selecting catchments in China

Area thresholds (km ²)	Number of catchments	R^2			Parameters (mm)		
		Q_s	Q_b	Q	W_p	V_p	U_p
2,000	67	0.85	0.62	0.89	3220	2794	1439
5,000	135	0.84	0.63	0.89	3004	2651	1356
10,000	180	0.84	0.69	0.90	3098	2614	1375
20,000	219	0.85	0.68	0.90	3138	2585	1376
80,000	257	0.85	0.69	0.90	3207	2487	1364
500,000	295	0.85	0.69	0.91	3278	2428	1362

665

带格式表格

带格式的：正文，行距：单倍行距

666 **Acknowledgments**

667 This research was supported by the National Natural Science Foundation of China (grant no.
668 42041004 and 52309022) and the China National Key R&D Program (grant nos.
669 2021YFC3000202 and 2022YFC3002802).

670 **Data and code Availability**

671 The CAMELS data set is available at <https://ral.ucar.edu/solutions/products/camels>. The
672 hydro-meteorological data of the catchments across China can be obtained from the Zenodo
673 repository via <https://zenodo.org/records/11058118> (Li et al., 2024).

674 **Reference**

675 Addor, N., Newman, A.J., Mizukami, N. & Clark, M.P. (2017). The CAMELS data set: catchment attributes and
676 meteorology for large-sample studies. *Hydrology and Earth System Sciences*, 21(10): 5293-5313.
677 DOI:10.5194/hess-21-5293-2017

678 Al-Ghobari, H., Dewidar, A. & Alataway, A. (2020). Estimation of Surface Water Runoff for a Semi-Arid Area Using RS
679 and GIS-Based SCS-CN Method. *Water*, 12(7). DOI:10.3390/w12071924

680 Beck, H.E., van Dijk, A., Miralles, D.G., de Jeu, R.A.M., Bruijnzeel, L.A., McVicar, T.R. & Schellekens, J. (2013). Global
681 patterns in base flow index and recession based on streamflow observations from 3394 catchments. *Water
Resources Research*, 49(12): 7843-7863. DOI:10.1002/2013wr013918

682 Berghuijs, W.R., Larsen, J.R., van Emmerik, T.H.M. & Woods, R.A. (2017). A Global Assessment of Runoff Sensitivity
683 to Changes in Precipitation, Potential Evaporation, and Other Factors. *Water Resources Research*, 53(10):
684 8475-8486. DOI:10.1002/2017wr021593

685 Beven, K.J. & Kirkby, M.J. (1979). A physically based, variable contributing area model of basin hydrology / Un
686 modèle à base physique de zone d'appel variable de l'hydrologie du bassin versant. *Hydrological Sciences
Bulletin*, 24(1): 43-69. DOI:10.1080/02626667909491834

687 Budyko, M.I., (1974). Climate and life: English Edited by Miller, D. H. Academic Press, New York.

688 Chen, S. & Ruan, X.H. (2023). A hybrid Budyko-type regression framework for estimating baseflow from climate and
689 catchment attributes. *Journal of Hydrology*, 618. DOI:10.1016/j.jhydrol.2023.129118

690 Cheng, S., Hulsman, P., Koppa, A., Beck, H.E., Cheng, L. & Miralles, D.G., (2023). Global runoff partitioning based on
691 Budyko-constrained machine learning. Zenodo. DOI:<https://doi.org/10.5281/ZENODO.7932122>

692 Cheng, S.J., Cheng, L., Liu, P., Qin, S.J., Zhang, L., Xu, C.Y., Xiong, L.H., Liu, L. & Xia, J. (2021). An Analytical Baseflow
693 Coefficient Curve for Depicting the Spatial Variability of Mean Annual Catchment Baseflow. *Water
Resources Research*, 57(8). DOI:10.1029/2020wr029529

694 Cheng, S.J., Cheng, L., Liu, P., Zhang, L., Xu, C.Y., Xiong, L.H. & Xia, J. (2020). Evaluation of baseflow modelling
695 structure in monthly water balance models using 443 Australian catchments. *Journal of Hydrology*, 591.
696 DOI:10.1016/j.jhydrol.2020.125572

700 Cheng, S.J., Cheng, L., Qin, S.J., Zhang, L., Liu, P., Liu, L., Xu, Z.C. & Wang, Q.L. (2022). Improved Understanding of
701 How Catchment Properties Control Hydrological Partitioning Through Machine Learning. *Water Resources*
702 *Research*, 58(4). DOI:10.1029/2021wr031412

703 Choudhury, B.J. (1999). Evaluation of an empirical equation for annual evaporation using field observations and
704 results from a biophysical model. *Journal of hydrology (Amsterdam)*, 216(1-2): 99-110.
705 DOI:10.1016/S0022-1694(98)00293-5

706 de Graaf, I.E.M., Gleeson, T., van Beek, L.P.H., Sutanudjaja, E.H., Bierkens, M.F.P., Hyologie, Landscape functioning, G.
707 & Hyology. (2019). Environmental flow limits to global groundwater pumping. *Nature*, 574(7776): 90-94.
708 DOI:10.1038/s41586-019-1594-4

709 Fan, Y., Li, H. & Miguez-Macho, G. (2013). Global Patterns of Groundwater Table Depth. *Science*, 339(6122): 940-943.
710 DOI:10.1126/science.1229881

711 Ficklin, D.L., Robeson, S.M. & Knouft, J.H. (2016). Impacts of recent climate change on trends in baseflow and
712 stormflow in United States watersheds. *Geophysical Research Letters*, 43(10): 5079-5088.
713 DOI:10.1002/2016gl069121

714 Gnann, S.J., (2021). Baseflow Generation at the Catchment Scale : an Investigation Using Comparative Hydrology.
715 Dissertation/Thesis Thesis.

716 Gnann, S.J., Woods, R.A. & Howden, N.J.K. (2019). Is There a Baseflow Budyko Curve? *Water Resources Research*,
717 55(4): 2838-2855. DOI:10.1029/2018wr024464

718 Hale, C.A., Carling, G.T., Nelson, S.T., Fernandez, D.P., Brooks, P.D., Rey, K.A., Tingey, D.G., Packer, B.N. & Aanderud, Z.T.
719 (2022). Strontium isotope dynamics reveal streamflow contributions from shallow flow paths during
720 snowmelt in a montane watershed, Provo River, Utah, USA. *Hydrological Processes*, 36(1).
721 DOI:10.1002/hyp.14458

722 Hall, F.R. (1968). BASE-FLOW RECESSIONS-A REVIEW. *Water Resources Research*, 4(5): 973-8.
723 DOI:10.1029/WR004i005p00973

724 Han, J.T., Yang, Y.T., Roderick, M.L., McVicar, T.R., Yang, D.W., Zhang, S.L. & Beck, H.E. (2020). Assessing the
725 Steady-State Assumption in Water Balance Calculation Across Global Catchments. *Water Resources*
726 *Research*, 56(7). DOI:10.1029/2020wr027392

727 Han, P.F., Sankarasubramanian, A., Wang, X.S., Wan, L. & Yao, L.L. (2023). One-Parameter Analytical Derivation in
728 Modified Budyko Framework for Unsteady-State Streamflow Elasticity in Humid Catchments. *Water*
729 *Resources Research*, 59(9). DOI:10.1029/2023wr034725

730 Harman, C.J., Troch, P.A. & Sivapalan, M. (2011). Functional model of water balance variability at the catchment
731 scale: 2. Elasticity of fast and slow runoff components to precipitation change in the continental United
732 States. *Water Resources Research*, 47. DOI:10.1029/2010wr009656

733 He, Y., Hu, Y.Y., Song, J.X. & Jiang, X.H. (2021). Variation of runoff between southern and northern China and their
734 attribution in the Qinling Mountains, China. *Ecological Engineering*, 171.
735 DOI:10.1016/j.ecoleng.2021.106374

736 He, Y., Yang, H., Liu, Z. & Yang, W. (2022). A framework for attributing runoff changes based on a monthly water
737 balance model: An assessment across China. *Journal of Hydrology*, 615: 128606.
738 DOI:<https://doi.org/10.1016/j.jhydrol.2022.128606>

739 He, Y., Yang, H. & Li, C. (2025). Long-term variations and regional disparities in baseflow during 1960 – 2021 across
740 China. *Journal of Hydrology*, 663: 134297. DOI:<https://doi.org/10.1016/j.jhydrol.2025.134297>

741 Hellwig, J. & Stahl, K. (2018). An assessment of trends and potential future changes in groundwater-baseflow
742 drought based on catchment response times. *Hydrology and Earth System Sciences*, 22(12): 6209-6224.
743 DOI:10.5194/hess-22-6209-2018

744 Horton, R.E. (1933). The role of infiltration in the hydrological cycle. *Eos, Transactions American Geophysical Union*,
745 14: 446–460.

746 Huang, M.B., Gallichand, J., Dong, C.Y., Wang, Z.L. & Shao, M.G. (2007). Use of soil moisture data and curve number
747 method for estimating runoff in the Loess Plateau of China. *Hydrological Processes*, 21(11): 1471-1481.
748 DOI:10.1002/hyp.6312

749 Huang, T., Yu, D., Cao, Q. & Qiao, J. (2019). Impacts of meteorological factors and land use pattern on hydrological
750 elements in a semi-arid basin. *Sci Total Environ*, 690: 932-943. DOI:10.1016/j.scitotenv.2019.07.068

751 Huang, Z., Yang, H. & Yang, D. (2016). Dominant climatic factors driving annual runoff changes at the catchment
752 scale across China. *Hydrology and earth system sciences*, 20(7): 2573-2587.
753 DOI:10.5194/hess-20-2573-2016

754 Kaleris, V. & Langousis, A. (2017). Comparison of two rainfall-runoff models: effects of conceptualization on water
755 budget components. *Hydrological Sciences Journal-Journal Des Sciences Hydrologiques*, 62(5): 729-748.
756 DOI:10.1080/02626667.2016.1250899

757 L'vovich, M.I., (1979). World water resources and their future. , Washington: American Geophysical Union.
758 DOI:<https://doi.org/10.1029/SP013>

759 Lee, S.H.Y. & Ajami, H. (2023). Comprehensive assessment of baseflow responses to long-term meteorological
760 droughts across the United States. *Journal of Hydrology*, 626. DOI:10.1016/j.jhydrol.2023.130256

761 Li, X., Zhang, K., Gu, P.R., Feng, H.T., Yin, Y.F., Chen, W. & Cheng, B.C. (2021). Changes in precipitation extremes in the
762 Yangtze River Basin during 1960-2019 and the association with global warming, ENSO, and local effects.
763 *Science of the Total Environment*, 760. DOI:10.1016/j.scitotenv.2020.144244

764 Li, Z., Huang, S., Liu, D., Leng, G., Zhou, S. & Huang, Q. (2020). Assessing the effects of climate change and human
765 activities on runoff variations from a seasonal perspective. *Stoch Environ Res Risk Assess*, 34(3-4): 575-592.
766 DOI:10.1007/s00477-020-01785-1

767 Liu, J.Y., Zhang, Q., Feng, S.Y., Gu, X.H., Singh, V.P. & Sun, P. (2019). Global Attribution of Runoff Variance Across
768 Multiple Timescales. *Journal of Geophysical Research-Atmospheres*, 124(24): 13962-13974.
769 DOI:10.1029/2019jd030539

770 Liu, Z., Yang, H. & Wang, T. (2021). A simple framework for estimating the annual runoff frequency distribution
771 under a non-stationarity condition. *Journal of hydrology (Amsterdam)*, 592: 125550.
772 DOI:10.1016/j.jhydrol.2020.125550

773 Lyne, V.D., Hollick, M., (1979). Stochastic time-variable rainfall runoff modelling. In *Hydrology and Water Resources
774 Symposium* (pp. 82–92). Institution of Engineers, Perth, Australia.

775 Mallakpour, I. & Villarini, G. (2017). Analysis of changes in the magnitude, frequency, and seasonality of heavy
776 precipitation over the contiguous USA. *Theoretical and Applied Climatology*, 130(1-2): 345-363.
777 DOI:10.1007/s00704-016-1881-z

778 Massoud, E.C., Lee, H., Gibson, P.B., Loikith, P. & Waliser, D.E. (2020). Bayesian Model Averaging of Climate Model
779 Projections Constrained by Precipitation Observations over the Contiguous United States. *Journal of
780 hydrometeorology*, 21(10): 2401-2418. DOI:10.1175/JHM-D-19-0258.1

781 Milly, P.C.D. & Dunne, K.A. (2002). Macroscale water fluxes 2. Water and energy supply control of their interannual
782 variability. *Water Resour. Res*, 38(10): 24-1-24-9. DOI:10.1029/2001WR000760

783 Morgan, R.P.C., Nearing, M. A. (Eds.). (2011). *Handbook of erosion modeling*. West Sussex: Wiley ~ Blackwell.

784 Neto, A.A.M., Roy, T., de Oliveira, P.T.S. & Troch, P.A. (2020). An Aridity Index-Based Formulation of Streamflow
785 Components. *Water Resources Research*, 56(9). DOI:10.1029/2020wr027123

786 Newman, A.J., Clark, M.P., Sampson, K., Wood, A., Hay, L.E., Bock, A., Viger, R.J., Blodgett, D., Brekke, L., Arnold, J.R.,
787 Hopson, T. & Duan, Q. (2015). Development of a large-sample watershed-scale hydrometeorological data

788 set for the contiguous USA: data set characteristics and assessment of regional variability in hydrologic
789 model performance. *Hydrology and Earth System Sciences*, 19(1): 209-223. DOI:10.5194/hess-19-209-2015

790 Ning, T., Feng, Q. & Qin, Y. (2022). Recent variations in the seasonality difference between precipitation and
791 potential evapotranspiration in China. *International journal of climatology*, 42(7): 3616-3632.
792 DOI:10.1002/joc.7435

793 Penman, H.L. (1948). Natural evaporation from open water, bare soil and grass. Proc. R. Soc. London Ser. Math. Phys.
794 Sci. 193 (1032), 120. DOI: <https://doi.org/10.1098/rspa.1948.0037>

795 Pimentel, R., Arheimer, B., Crochemore, L., Andersson, J. C. M., Pechlivanidis, I. G. & Gustafsson, D. (2023). Which
796 Potential Evapotranspiration Formula to Use in Hydrological Modeling World - Wide? Water resources
797 research, 59(5). DOI:10.1029/2022WR033447

798 Ponce, V.M. & Shetty, A.V. (1995). A CONCEPTUAL-MODEL OF CATCHMENT WATER-BALANCE .1. FORMULATION AND
799 CALIBRATION. *Journal of Hydrology*, 173(1-4): 27-40. DOI:10.1016/0022-1694(95)02739-c

800 Price, K., Jackson, C.R., Parker, A.J., Reitan, T., Dowd, J. & Cyterski, M. (2011). Effects of watershed land use and
801 geomorphology on stream low flows during severe drought conditions in the southern Blue Ridge
802 Mountains, Georgia and North Carolina, United States. *Water Resources Research*, 47.
803 DOI:10.1029/2010wr009340

804 Roderick, M.L. & Farquhar, G.D. (2011). A simple framework for relating variations in runoff to variations in climatic
805 conditions and catchment properties. *Water Resour. Res*, 47(12): n/a. DOI:10.1029/2010WR009826

806 Schaake, J.C., (1990). From climate to flow, in: climate change and U.S. water resources, edited by: Waggoner, P. E.,
807 chap. 8. John Wiley, New York.

808 Schiavo, M. (2023). The role of different sources of uncertainty on the stochastic quantification of subsurface
809 discharges in heterogeneous aquifers. Journal of Hydrology, 617: 128930.
810 DOI:10.1016/j.jhydrol.2022.128930

811 SCS, (1972). National Engineering Handbook, section 4. Soil Conservation Service USDA, Washington, DC.

812 Shen, Y. & Xiong, A.Y. (2016). Validation and comparison of a new gauge-based precipitation analysis over mainland
813 China. *International Journal of Climatology*, 36(1): 252-265. DOI:10.1002/joc.4341

814 Shi, W., Huang, M., Gongadze, K. & Wu, L. (2017). A Modified SCS-CN Method Incorporating Storm Duration and
815 Antecedent Soil Moisture Estimation for Runoff Prediction. *Water Resources Management*, 31(5):
816 1713-1727. DOI:<https://doi.org/10.1007/s11269-017-1610-0>

817 Singh, S.K., Pahlow, M., Booker, D.J., Shankar, U. & Chamorro, A. (2019). Towards baseflow index characterisation at
818 national scale in New Zealand. *Journal of Hydrology*, 568: 646-657. DOI:10.1016/j.jhydrol.2018.11.025

819 Sivapalan, M., Yaeger, M.A., Harman, C.J., Xu, X.Y. & Troch, P.A. (2011). Functional model of water balance variability
820 at the catchment scale: 1. Evidence of hydrologic similarity and space-time symmetry. *Water Resources*
821 *Research*, 47. DOI:10.1029/2010wr009568

822 Sun, Y., Tian, F.Q., Yang, L. & Hu, H.P. (2014). Exploring the spatial variability of contributions from climate variation
823 and change in catchment properties to streamflow decrease in a mesoscale basin by three different
824 methods. *Journal of Hydrology*, 508: 170-180. DOI:10.1016/j.jhydrol.2013.11.004

825 Troch, P.A., Martinez, G.F., Pauwels, V.R.N., Durcik, M., Sivapalan, M., Harman, C., Brooks, P.D., Gupta, H. & Huxman,
826 T. (2009). Climate and vegetation water use efficiency at catchment scales. *Hydrological Processes*, 23(16):
827 2409-2414. DOI:10.1002/hyp.7358

828 Wallace, S., Biggs, T., Lai, C.-T. & McMillan, H. (2021). Tracing sources of stormflow and groundwater recharge in an
829 urban, semi-arid watershed using stable isotopes. *Journal of Hydrology: Regional Studies*, 34: 100806.
830 DOI:<https://doi.org/10.1016/j.ejrh.2021.100806>

831 Wang, D. & Wu, L. (2013). Similarity of climate control on base flow and perennial stream density in the Budyko

带格式的: 超链接
带格式的: 超链接

832 framework. *Hydrology and earth system sciences*, 17(1): 315-324. DOI:10.5194/hess-17-315-2013

833 Wang, H., Liu, J., Klaar, M., Chen, A., Gudmundsson, L. & Holden, J. (2024). Anthropogenic climate change has
834 influenced global river flow seasonality. *Science (New York, N.Y.)*, 383(6686): 1009-1014.
835 DOI:10.1126/science.adi9501

836 [Wang, K., Bai, P. & Liu, X. \(2025\). Three Paradoxes Related to Potential Evapotranspiration in a Warming Climate. Current climate change reports, 11\(1\):6. DOI:10.1007/s40641-025-00203-4](#)

838 Wu, J.W., Miao, C.Y., Duan, Q.Y., Lei, X.H., Li, X.Y. & Li, H. (2019). Dynamics and Attributions of Baseflow in the
839 Semiarid Loess Plateau. *Journal of Geophysical Research-Atmospheres*, 124(7): 3684-3701.
840 DOI:10.1029/2018jd029775

841 Wu, S., Zhao, J., Wang, H. & Sivapalan, M. (2021). Regional Patterns and Physical Controls of Streamflow Generation
842 Across the Conterminous United States. *Water resources research*, 57(6): n/a. DOI:10.1029/2020WR028086

843 Wu, Y.Y., Fang, H.W., Huang, L. & Ouyang, W. (2020). Changing runoff due to temperature and precipitation
844 variations in the dammed Jinsha River. *Journal of Hydrology*, 582. DOI:10.1016/j.jhydrol.2019.124500

845 Xu, F., Zhou, Y.Y. & Zhao, L.L. (2022). Spatial and temporal variability in extreme precipitation in the Pearl River Basin,
846 China from 1960 to 2018. *International Journal of Climatology*, 42(2): 797-816. DOI:10.1002/joc.7273

847 Xu, X.Y., Yang, D.W., Yang, H.B. & Lei, H.M. (2014). Attribution analysis based on the Budyko hypothesis for detecting
848 the dominant cause of runoff decline in Haihe basin. *Journal of Hydrology*, 510: 530-540.
849 DOI:10.1016/j.jhydrol.2013.12.052

850 Yang, H.B., Qi, J., Xu, X.Y., Yang, D.W. & Lv, H.F. (2014). The regional variation in climate elasticity and climate
851 contribution to runoff across China. *Journal of Hydrology*, 517: 607-616. DOI:10.1016/j.jhydrol.2014.05.062

852 Yang, H.B., Yang, D.W., Lei, Z.D. & Sun, F.B. (2008). New analytical derivation of the mean annual water-energy
853 balance equation. *Water Resources Research*, 44(3). DOI:10.1029/2007wr006135

854 Yang, W.T., Long, D. & Bai, P. (2019). Impacts of future land cover and climate changes on runoff in the mostly
855 afforested river basin in North China. *Journal of Hydrology*, 570: 201-219.
856 DOI:10.1016/j.jhydrol.2018.12.055

857 Yao, L.L., Sankarasubramanian, A. & Wang, D.B. (2021). Climatic and Landscape Controls on Long-Term Baseflow.
858 *Water Resources Research*, 57(6). DOI:10.1029/2020wr029284

859 Ye, X., Xu, C., Zhang, D. & Li, X. (2018). Variation of Summer Precipitation and Its Connection with Asian Monsoon
860 System in the Middle-lower Yangtze River Basin. *Scientia Geographica Sinica*, 38(7): 1174-1182.

861 Yin, J.B., Gentile, P., Zhou, S., Sullivan, S.C., Wang, R., Zhang, Y. & Guo, S.L. (2018). Large increase in global storm
862 runoff extremes driven by climate and anthropogenic changes. *Nature Communications*, 9.
863 DOI:10.1038/s41467-018-06765-2

864 Zhang, D., (2015). On the effects of seasonality of precipitation and potential evapotranspiration on catchment
865 hydrologic partitioning., Tsinghua University, Beijing, China, p. 150. pp.

866 Zhang, J.L., Zhang, Y.Q., Song, J.X. & Cheng, L. (2017). Evaluating relative merits of four baseflow separation methods
867 in Eastern Australia. *Journal of Hydrology*, 549: 252-263. DOI:10.1016/j.jhydrol.2017.04.004

868 Zheng Mingguo, S.L. (2014). Recent change of runoff and its components of baseflow and surface runoff in response
869 to climate change and human activities for the Lishui watershed of southern China (in Chinese).
870 *Geographical Research*, 33(02): 237-250.

871 [Zuecco, G., Rinderer, M., Penna, D., Borga, M. & van Meerveld, H.J. \(2019\). Quantification of subsurface
872 hydrologic connectivity in four headwater catchments using graph theory. The Science of the total
873 environment, 646:1265-1280. DOI:10.1016/j.scitotenv.2018.07.269](#)